viruses

MDPI

Article

SARS-CoV-2 Delta Variant Displays Moderate Resistance to Neutralizing Antibodies and Spike Protein Properties of Higher Soluble ACE2 Sensitivity, Enhanced Cleavage and Fusogenic Activity

Sabari Nath Neerukonda [1], Russell Vassell [1], Sabrina Lusvarghi [1], Richard Wang [1], Fernando Echegaray [2], Lisa Bentley [3], Ann E. Eakin [4], Karl J. Erlandson [5], Leah C. Katzelnick [2], Carol D. Weiss [1,*] and Wei Wang [1,*]

1 Division of Viral Products, Office of Vaccines Research and Review, Center for Biologics Evaluation and Research, U.S. Food and Drug Administration, Silver Spring, MD 20903, USA; NagaVenka.Neerukonda@fda.hhs.gov (S.N.N.); Russell.Vassell@fda.hhs.gov (R.V.); Sabrina.Lusvarghi@fda.hhs.gov (S.L.); Richard.Wang@fda.hhs.gov (R.W.)
2 Viral Epidemiology and Immunity Unit, Laboratory of Infectious Diseases, National Institute of Allergy and Infectious Diseases, National Institutes of Health, Bethesda, MD 20892, USA; fernando.echegaray@nih.gov (F.E.); leah.katzelnick@nih.gov (L.C.K.)
3 Office of the Assistance Secretary for Preparedness and Response, U.S. Department of Health and Human Services, Washington, DC 20201, USA; LisaMarie.Bentley@hhs.gov
4 Division of Microbiology and Infectious Diseases, National Institute of Allergy and Infectious Disease, National Institutes of Health, Rockville, MD 20892, USA; ann.eakin@nih.gov
5 Influenza and Emerging Infectious Diseases Division, Biomedical Advanced Research and Development Authority, U.S. Department of Health and Human Services, Washington, DC 20201, USA; Karl.Erlandson@hhs.gov
* Correspondence: carol.weiss@fda.hhs.gov (C.D.W.); wei.wang@fda.hhs.gov (W.W.)

Abstract: The SARS-CoV-2 B.1.617 lineage variants, Kappa (B.1.617.1) and Delta (B.1.617.2, AY) emerged during the second wave of infections in India, but the Delta variants have become dominant worldwide and continue to evolve. Here, we compared B.1.617 variants for neutralization resistance by convalescent sera, mRNA vaccine-elicited sera, and therapeutic neutralizing antibodies using a pseudovirus neutralization assay. B.1.617.1, B.1.617.2, and AY.1 pseudoviruses showed a modest 1.5- to 4.4-fold reduction in neutralization by convalescent sera and vaccine-elicited sera. In comparison, similar modest reductions were also observed for C.37, P.1, R.1, and B.1.526 pseudoviruses, but 7- and 16-fold reductions for vaccine-elicited and convalescent sera, respectively, were seen for B.1.351 pseudoviruses. Among twenty-three therapeutic antibodies tested, four antibodies showed either complete or partial loss of neutralization against B.1.617.2 pseudoviruses and six antibodies showed either complete or partial loss of neutralization against B.1.617.1 and AY.1 pseudoviruses. Our results indicate that the current mRNA-based vaccines will likely remain effective in protecting against B.1.617 variants. Finally, the P681R substitution confers efficient cleavage of B.1.617 variants' spike proteins and the spike of Delta variants exhibited greater sensitivity to soluble ACE2 neutralization, as well as fusogenic activity, which may contribute to enhanced spread of Delta variants.

Keywords: SARS-CoV-2; B.1.617 variants; neutralizing antibodies; neutralization resistance; spike cleavage; syncytia formation; antigenic distance

Citation: Neerukonda, S.N.; Vassell, R.; Lusvarghi, S.; Wang, R.; Echegaray, F.; Bentley, L.; Eakin, A.E.; Erlandson, K.J.; Katzelnick, L.C.; Weiss, C.D.; et al. SARS-CoV-2 Delta Variant Displays Moderate Resistance to Neutralizing Antibodies and Spike Protein Properties of Higher Soluble ACE2 Sensitivity, Enhanced Cleavage and Fusogenic Activity. *Viruses* **2021**, *13*, 2485. https://doi.org/10.3390/v13122485

Academic Editor: Shibo Jiang

Received: 29 October 2021
Accepted: 8 December 2021
Published: 11 December 2021

1. Introduction

Since its origin in December 2019, severe acute respiratory syndrome coronavirus 2 (SARS-CoV-2) has spread globally to cause a coronavirus disease 2019 (COVID-19) pandemic that recorded more than 263 million infections and has claimed 5.2 million lives thus far (Johns Hopkins Coronavirus Resource Center; https://coronavirus.jhu.edu,

accessed date: 1 December 2021). SARS-CoV-2 trimeric spike (S) glycoprotein on the virion surface binds the angiotensin-converting enzyme (ACE2) to facilitate cellular entry and is the target of therapeutic neutralizing antibodies and vaccines [1–6]. The spike is proteolytically processed between R^{685} | S^{686} into S1 and S2 subunits, which facilitates subsequent cleavage at the S2′ site (R^{815} | S^{816}) by TMPRSS2 for viral entry into respiratory cells. The S1 subunit spans the N-terminal domain (NTD) and the receptor-binding domain (RBD) within the C-terminal domain (CTD) whereas the S2 subunit spans the fusion peptide and a linker region flanked by heptad repeat regions that drive virus-cell membrane fusion [7]. Besides virus-cell fusion, spike protein on the cell surface can trigger receptor-dependent syncytia formation via cell-cell fusion.

Currently, available vaccines and therapeutic antibodies target the spike glycoprotein of an early isolate of SARS-CoV-2. The continued evolution of SARS-CoV-2 resulted in the emergence of several variants of distinct lineages globally, raising concerns over variant transmissibility and immune escape. One of the earliest variants that is highly infectious and thus became globally dominant is B.1 (D614G) [8–11]. However, convalescent sera from individuals infected with an early viral isolate (Wuhan-Hu-1) effectively cross-neutralized D614G [12]. Subsequent genomic surveillance has led to the identification of several convergently evolving lineages, including in UK—B.1.1.7 (Alpha), South Africa—B.1.351 (Beta), Brazil/Japan—P.1 (Gamma), California, USA—B.1.427/B.1.429 (Epsilon), Northeast USA—B.1.526 (Iota), USA/Japan—(R.1), Peru/Chile—C.37 (Lambda), and Liverpool—A.23.1. By late 2020, B.1.617 lineage variants emerged in India and have spread rapidly throughout the world. The Kappa (B.1.617.1) variant emerged early in the second wave, followed by the Delta (B.1.617.2) and its sublineage (AY.1 and AY.2) variants, which are currently dominant in many parts of the world.

Several key substitutions in the RBD of spike were demonstrated to either enhance affinity towards ACE2 or contribute to immune escape. The E484K substitution in the RBD of B.1.351, P.1, R.1, and B.1.526 variants was previously identified among in vitro escape mutants selected against single antibody and antibody cocktails [13,14]. Several studies have described a significant drop in the neutralization potency of convalescent and vaccine sera, as well as numerous therapeutic neutralizing antibodies that contacted the mutated sites in B.1.351, P.1, and B.1.526 lineages, particularly E484K [15–22]. The B.1.427/B.1.429 and B.1.617 lineage variants share the L452R substitution in RBD [23]. The L452R substitution has been demonstrated to enhance ACE2 binding and pseudovirus infectivity [24] and reduce or ablate the neutralizing potency of 10 out of 34 RBD-specific mAbs tested [23]. The E484Q along with L452R is present in the RBD of B.1.617 sublineages, B.1.617.1 and B.1.617.3. B.1.617.1 contains additional substitutions in the NTD (T95I), the NTD antigenic supersite β-hairpin (G142D and E154K), within the S1/S2 cleavage junction (P681R), and in the S2 subunit (Q1071H) [25]. E484Q was also previously identified as an RBD escape mutant for an RBD-specific mAb [26,27].

The spike protein of the B.1.617.2 variant contains nine substitutions and deletions compared to the early D614G variant used here as wild type (WT or D614G). The three substitutions (T19R, G142D, and R158G) and two deletions (ΔE156, ΔF157) in NTD occur in the NTD antigenic supersite spanning between residues 14–20, 140–158, and 245–264 [27]. In addition, the B.1.617.2 spike also has two substitutions in the receptor-binding domain (RBD) (L452R, T478K), one substitution proximal to S1/S2 cleavage site (P681R), and one in the S2 region (D950N). An additional substitution in RBD, K417N is also observed in the RBD of AY.1. The L452R RBD substitution was shown to confer modest resistance to neutralization by convalescent sera, vaccine-elicited sera, and therapeutic neutralizing antibodies in the context of other variants of interest (VOI), such as B.1.427/B.1.429 and B.1.617.1 [23,24]. The E484K substitution found in B.1.351, B.1.526, P.1, P.3 (theta), and some B.1.617 variants confers some level of resistance to neutralization by convalescent sera, vaccine-elicited sera, and therapeutic neutralizing antibodies [16]. In addition to neutralizing antibody resistance, spike mutations affect proteolytic processing, virion incorporation, and ACE2 affinity, as well as membrane fusion [28–30].

The global dominance and ongoing evolution of B.1.617 lineage variants require continuing assessment of the neutralization potency of convalescent sera, vaccine-elicited sera, and therapeutic neutralizing antibodies against emerging B.1.617 variants. Here, we measured the neutralization potency of convalescent sera, vaccine-elicited sera, and therapeutic neutralizing antibodies against two independent variants each in the Kappa (B.1.617.1) and Delta (B.1.617.2, AY.1) lineages and assessed the contribution of the RBD substitutions in conferring resistance. We found that resistance to convalescent and vaccine-elicited sera was predominantly conferred by RBD substitutions E484Q, T478K, and L452R. Furthermore, out of 23 therapeutic neutralizing antibodies tested, Kappa and Delta pseudoviruses displayed complete resistance to five neutralizing antibodies and partial resistance to one antibody. Finally, we showed that the P681R substitution confers enhanced furin processing in spike protein of B.1.617 lineage variants that corresponded to enhanced cell-cell fusion activity. However, only Delta spike protein exhibited greater sensitivity to soluble ACE2 inhibition, implying enhanced ACE2 affinity. This feature along with enhanced cell-cell fusion activity may contribute to the dominance of the B.1.617.2 variant.

2. Materials and Methods

2.1. Ethics Statement

Use of de-identified sera in this study was approved by the U.S. Food and Drug Administration Research in Human Subjects Committee. Vaccine-elicited sera were collected at the U.S. Food and Drug Administration with written consent under an approved Institutional Review Board (IRB) protocol (FDA IRB Study # 2021-CBER-045).

2.2. Plasmids and Cell Lines

Codon-optimized full-length open reading frames of the S genes of SARS-CoV-2 variants were cloned into pcDNA3.1(+) or pVRC8400 by GenScript (Piscataway, NJ, USA). The codon optimization for gene expression in human cell was performed by GenScript's OptimumGene algorithm system to optimize the following parameters: codon usage bias, GC content, CpG dinucleotides content, mRNA secondary structure, internal chi sites and ribosomal binding sites, negative CpG islands, cryptic splicing sites, premature PolyA sites, PolyT sites, RNA instability motif (ARE), and repeat sequences (direct repeat, reverse repeat). The codon-optimized sequence of Wuhan-Hu-1 S gene is shown in Supplementary Figure S1. The spikes of variants used in this study are listed in Table 1. The HIV gag/pol (pCMVΔR8.2), and luciferase reporter (pHR'CMV-Luc) plasmids were obtained from the Vaccine Research Center (National Institutes of Health, Bethesda, MD, USA) [31,32]. 293T-ACE2.TMPRSS2 cells stably expressing human angiotensin-converting enzyme 2 (ACE2) and transmembrane serine protease 2 (TMPRSS2) were previously described (BEI Resources, Manassas, VA, USA; Cat no: NR-55293) [33]. The 293T and 293T-ACE2.TMPRSS2 cells were maintained at 37 °C in Dulbecco's modified eagle medium (DMEM) supplemented with high glucose, L-glutamine, minimal essential media (MEM) non-essential amino acids, penicillin/streptomycin, and 10% fetal bovine serum (FBS).

2.3. Human Sera and Therapeutic Neutralizing Antibodies

Convalescent sera from SARS-CoV-2-infected donors (n = 10) collected 6–61 days after symptom onset were purchased from Bocabiolistics (Pompano Beach, FL, USA). Donors were 18–73 years old with six males/four females. The information about the convalescent sera is shown in Table 2. Sera from Pfizer/BioNtech BNT162b2 (n = 15) or Moderna mRNA-1273 vaccinated individuals (n = 14) obtained two weeks after the second vaccination were used in this study. Vaccinated individual donors were 21–65 years old with six males/nine females for Pfizer BNT162b2 vaccination and eight males/six females for Moderna mRNA-1273 vaccination. All sera were tested negative for non-specific neutralization using amphotropic murine leukemia enveloped pseudovirus. Vaccinated donors were prescreened for absence of both history of SARS-CoV-2 infection and SARS-CoV-2 neutralizing antibodies prior to vaccination. Twenty-three therapeutic neutralizing antibodies

against SARS-CoV-2 spike protein were donated by different pharmaceutical companies for the U.S. government COVID-19 response Therapeutics Research Team efforts to define neutralization profiles against existing and emerging SARS-CoV-2 variants [19]. Due to a confidentiality agreement with the manufacturers, neutralizing antibodies described are shown with blinded identification codes as follows: single neutralizing antibodies (nAbs A to R), combination of two neutralizing antibodies (cnAbs S to X), and polyclonal neutralizing antibodies (pnAbs III to IV).

Table 1. List of spike variants used in the present study.

Variants	Name Used in This Report	Amino Acid Substitutions in Spike Compared to Wuhan-Hu-1	RBD Substitutions
Wuhan-Hu-1	Wuhan-Hu-1		
Wuhan-Hu-1-PP681R	Wuhan-Hu-1 + P681R	P681R	
B.1	WT(D614G)	D614G	
B.1-P681R	P681R	D614G, P681R	
B.1-P681H	P681H	D614G, P681H	
B.1-L452R	L452R	L452R, D614G	L452R
B.1-E484Q	E484Q	E484Q, D614G	E484Q
B.1-T478K	T478K	T478K, D614G	T478K
B.1-K417N	K417N	K417N, D614G	K417N
B.1-L452R-T478K	L452R + T478K	L452R, T478K, D614G	L452R, T478K
B.1-L452Q-F490S	L452Q + F490S	L452Q, F490S, D614G	L452Q, F490S
B.1.617.1 (Kappa)	B.1.617.1 (A)	G142D, E154K, V382L, L452R, E484Q, D614G, P681R, Q1071H, D1153Y	V382L, L452R, E484Q
B.1.617.1 (Kappa)	B.1.617.1 (B)	T95I, G142D, E154K, L452R, E484Q, D614G, P681R, Q1071H	L452R, E484Q
B.1.617.2 (Delta)	B.1.617.2	T19R, G142D, E156Δ, F157Δ, R158G, L452R, T478K, D614G, P681R, D950N	L452R, T478K
AY.1 (Delta plus)	AY.1	T19R, T95I, G142D, E156Δ, F157Δ, R158G, W258L, K417N, L452R, T478K, D614G, P681R, D950N	K417N, L452R, T478K
C.37 (Lambda)	C.37	G75V, T76I, Δ246-252, D253N, L452Q, F490S, D614G, T859N	L452Q, F490S
B.1.429 (Epsilon)	B.1.429	S13I, P26S, W152C, L452R, D614G	L452R
R.1	R.1	W152L, E484K, D614G, G769V	E484K
B.1.526 (Iota)	B.1.526	L5F, T95I, D253G, E484K, D614G, A701V	E484K
P.1 (Gamma)	P.1	L18F, T20N, P26S, D138Y, R190S, K417T, E484K, N501Y, D614G, H655Y, T1027I, V1176F	K417T, E484K, N501Y
B.1.1.7 (Alpha)	B.1.1.7	69-70Δ, Y144Δ, N501Y, A570D, D614G, P681H, T716I, S982A, D1118H	N501Y
B.1.351 (Beta)	B.1.351	L18F, D80A, D215G, 241-243Δ, K417N, E484K, N501Y, D614G, A701V	K417N, E484K, N501Y

Table 2. Demographics and infection history of convalescent sera donor individuals.

Donor ID	Gender	Age	Days from 1st Symptoms	Residue Substitutions in Spike of SARS-CoV-2-Infected Individual
1	Male	36	16	D614G
2	Female	29	28	D614G
3	Male	70	14	D614G
4	Female	54	61	D614G
5	Male	18	13	D614G
6	Male	59	9	D614G
7	Male	25	40	S13I, Q52R, A67V, 69-70del, 144del, L452R
8	Female	73	59	L452R, D614G
9	Female	33	26	L452R, D614G
10	Male	55	6	W152C, L452R, D614G

2.4. Soluble ACE2 Production

His-tagged soluble ACE2 was produced in FreeStyle™ 293-F cells and purified using HisPur™ Ni-NTA Resin (Thermo Scientific, Waltham, MA, USA) as described previously [34].

2.5. SARS-CoV-2 Pseudovirus Production and Neutralization Assay

HIV-based lentiviral pseudoviruses with spike proteins were generated as previously described [33]. The B.1 spike containing D614G was used as wild type (WT(D614G)). Briefly, pseudoviruses bearing the spike glycoprotein and packaging a firefly luciferase (FLuc) reporter gene were produced in 293T cells by co-transfection of 5 µg of pCMVΔR8.2, 5 µg of pHR'CMVLuc and 4 µg of pcDNA3.1(+) or 0.5 µg of pVRC8400 encoding a codon-optimized spike gene with the desired substitutions. Pseudovirus supernatants were collected approximately 48 h post transfection, filtered through a 0.45 µm low protein binding filter, and stored at −80 °C. Neutralization assays were performed using 293T-ACE2.TMPRSS2 cells in 96-well plates as previously described [33]. Briefly, pseudoviruses with titers of approximately 1×10^6 relative luminescence units (RLU)/mL of luciferase activity were incubated with serially diluted sera or antibodies for two h at 37 °C. Pseudovirus and serum or antibody mixtures (100 µL) were then inoculated onto the plates pre-seeded one day earlier with 3.0×10^4 cells/well. Pseudovirus infectivity was scored 48 h later for luciferase activity. The antibody concentration or inverse of the sera dilutions causing a 50% reduction of RLU compared to control was reported as the neutralization titer. Titers were calculated using a nonlinear regression curve fit (GraphPad Prism Software Inc., La Jolla, CA, USA). The mean titer from at least two independent experiments each with intra-assay duplicates was reported as the final titer. WT(D614G) pseudovirus was run as a control for every assay.

For ACE2 neutralization assay, serially diluted recombinant human soluble ACE2 was incubated with indicated pseudovirus (~1×10^6 RLU/mL) for one hour at 37 °C and 100 µL of pseudovirus and soluble ACE2 mixture was added to 293T-ACE2.TMPRSS2 cells. Luciferase activity was measured 48 h later. The soluble ACE2 concentration causing a 50% reduction of RLU compared to control was reported as the 50% inhibitory concentration or IC_{50}.

2.6. Western Blotting

In total, 1.25 mL of pseudoviruses was pelleted at 4 °C for 2 h at 15,000 rpm using Tomy TX-160 ultracentrifuge. Pseudovirus pellet was resuspended in 1× Laemmli loading buffer and heated at 70 °C for 10 min. Samples were resolved by 4–20% SDS PAGE and transferred onto nitrocellulose membranes. Membranes were probed for SARS-CoV-2 S1 using rabbit polyclonal antibodies against the RBD domain (Sino Biological, Wayne, PA, USA).

2.7. Cell-Cell Fusion Assay

For measuring spike-protein-mediated cell-cell fusion, β-gal complementation assay was performed as described previously [35]. Briefly, β-gal ω subunit-expressing 293T cells were transfected with 1 µg spike plasmids, whereas 293T-ACE2.TMPRSS2 cells were transfected with β-gal α subunit using the Fugene 6 reagent. At 24 h post transfection, the transfected cells were detached using a nonenzymatic cell dissociation solution (Sigma, St. Louis, MO, USA) and washed with DMEM. Spike-transfected/β-gal ω subunit-expressing 293T cells were mixed with β-gal α subunit-transfected/293T-ACE2.TMPRSS2 cells at 1:1 ratio to a total of 6×10^4 cells per well on a 96-well plate. The cells were co-cultivated for 24 h at 37 °C. The culture supernatants were then removed, and cell-cell fusion was scored by determination of the β-gal activity in co-cultured cell lysates using a Galacto-Star kit (Applied Biosystems, Waltham, MA, USA) according to the manufacturer's instructions.

To ensure equivalent amount of spike cell surface expression levels among treatments, spike-transfected β-gal ω subunit-expressing 293T cells were quantified for cell surface

spike levels by flow cytometry. Spike-transfected 293T cells employed in cell-cell fusion assay were concurrently stained with SARS-CoV-2 positive human polyclonal sera at 1:20 dilution, washed twice, and then incubated with FITC-conjugated goat anti-human (KPL Inc., Gaithersburg, MD, USA). The cells were washed twice and then fixed with 2% paraformaldehyde. The results were acquired using BD LSRFortessa™ X-20 Cell Analyzer (BD Biosciences, San Jose, CA, USA). The mean fluorescence intensities of spike positive cells were recorded.

2.8. Antigenic Cartography

We created a geometric interpretation of neutralization titers against the tested SARS-CoV-2 pseudoviruses using Racmacs antigenic cartography software (Sam Wilks (2021), Racmacs: R Antigenic Cartography Macros. R package version 1.1.16. https://github.com/acorg/Racmacs, accessed on: 15 October 2021) [36,37]. The map is presented on a grid in which each square indicates one antigenic unit, corresponding to a two-fold dilution of the antibody in the neutralization assay. Antigenic distance is measured in any direction on the map.

2.9. Furin Prediction Score Calculations

The prediction of furin-specific cleavage site in spike proteins was computed using the ProP 1.0 Server hosted at http://www.cbs.dtu.dk/services/ProP/ (accessed on: 15 July 2021) and the PiTou V3 software hosted at http://www.nuolan.net/reference.html (accessed on: 15 July 2021).

2.10. Statistics Analysis

One-way analysis of variance (ANOVA) with Dunnett's multiple comparisons tests (variants compared to WT(D614G)), Mann–Whitney test for the comparison of two groups with unmatched pairs (Pfizer BNT162b2 compared to Moderna) and geometric mean titers (GMT) with 95% confidence intervals were performed using GraphPad Prism software. The p values of less than 0.05 were considered statistically significant. All neutralization titers were $\log_2$ transformed for analyses.

3. Results and Discussion

3.1. Neutralization of B.1.617 Pseudoviruses by Convalescent Sera

We first investigated the cross-neutralization potency of convalescent sera from individuals infected with SARS-CoV-2 in the U.S. against pseudoviruses bearing spikes of B.1.617.1 and B.1.617.2 variants and their corresponding RBD mutations (Figure 1A). Titers against B.1.617.1 (B), AY.1, E484Q, and L452R + T478K pseudoviruses were significantly different from the titers against WT(D614G). Compared to titers against WT(D614G) pseudoviruses (GMT 392), titers against B.1.617.1 (B) pseudoviruses were approximately four-fold lower (GMT 90), confirming and extending other reports [25,38,39]. Neutralization titers against WT(D614G) and L452R pseudoviruses were comparable (GMT titers 392 and 364, respectively), while neutralization titers against E484Q pseudoviruses were lower (GMT 165). Titers against B.1.617.2 (GMT 259) and AY.1 (GMT 203) pseudoviruses also showed a 1.5- and 1.9-fold reduction, respectively, compared to WT(D614G) pseudoviruses. Against pseudoviruses bearing spikes with T478K substitution in RBD, neutralization titers (GMT 270) were also reduced compared to WT(D614G) (GMT 392). A further reduction in neutralization titers was seen against pseudoviruses bearing both L452R and T478 substitutions in RBD displayed (GMT 192) compared to WT(D614G) (GMT 392).

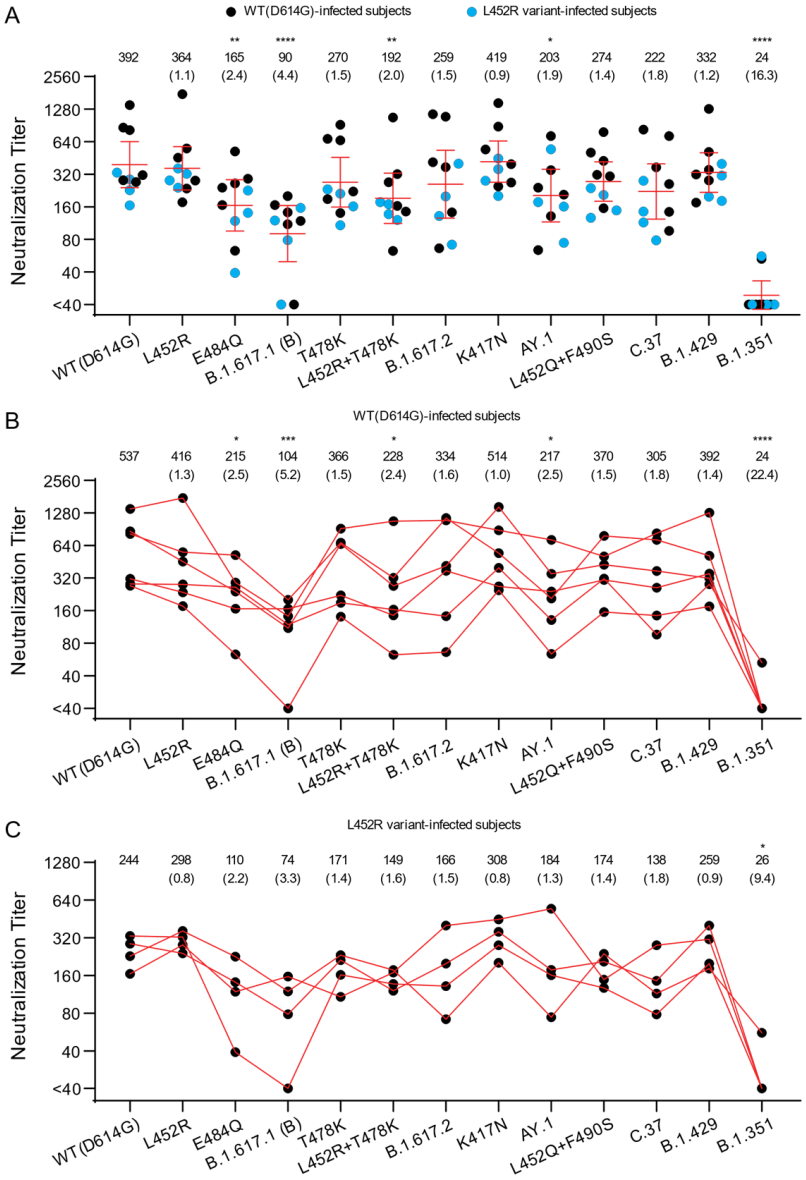

Figure 1. Neutralization of variant SARS-CoV-2 pseudoviruses by convalescent sera. The neutralization titers represented as 50% inhibitory concentrations (IC_{50}) against pseudoviruses bearing spike proteins from the indicated variants are plotted. (**A**) Individual neutralization titers of convalescent sera are presented. Blue dots: sera from subjects infected with variants containing L452R in spike. Black dots: sera from subjects infected with WT(D614G) variants. (**B**) The neutralization titers of individuals infected with WT(D614G) SARS-CoV-2. (**C**) The neutralization titers of individuals infected with SARS-CoV-2 bearing L452R in spike. The numbers over each graph indicate the GMT. The numbers in parentheses are the ratios of WT(D614G) GMT/individual variant GMT. p values were calculated by one-way analysis of variance (ANOVA) with Dunnett's multiple comparisons tests (variants compared to WT(D614G)). Titers measuring below the lowest serum dilution of 1:40 were treated as 20 for statistical analysis. All neutralization titers were $\log_2$ transformed before test. Bars: geometric means of titers (GMT) with %95 CI. *: $p \leq 0.05$; **: $p \leq 0.01$; ***: $p \leq 0.001$; ****: $p \leq 0.0001$.

The C.37 variant also has a substitution at L452 residue (L452Q instead of L452R) along with F490S in the RBD. A modest 1.8-fold reduction in titers against C.37 pseudoviruses was observed compared to WT(D614G) pseudoviruses (GMT titers 222 and 392, respectively). A 1.4-fold reduction in titers was observed for pseudoviruses with only the L452Q and F490S substitutions, indicating that these RBD substitutions contribute to C.37 resis-

tance. These findings are in agreement with a prior report showing a 3.3-fold reduction of convalescent sera neutralization titer for C.37 pseudoviruses compared to WT(D614G), as well as L452Q and F490S single substitutions contributing to neutralization resistance [40]. In comparison with other variants, we found that titers against B.1.429 pseudoviruses (GMT 332) were comparable to WT(D614G), but titers against the B.1.351 pseudovirus were 16.3-fold reduced (GMT 24) compared to WT(D614G), consistent with prior reports showing marked reductions of cross-neutralization against this variant [16–18,21].

Because the convalescent sera came from individuals who were previously infected by different variants (Table 2), we also explored differences in the neutralization titers between those infected by D614G variants lacking L452R and those infected by variants containing L452R (all have L452R and D614G, except one lacking D614G). The small number of samples in each group precludes conclusions, but we noticed modest differences against some variants. In the group infected by D614G variants that lacked L452R, a 5.2-fold, 1.6-fold, and 2.5-fold reduction in cross-neutralization potency was seen against B.1.617.1 (B), B.1.617.2, and AY.1 pseudoviruses, respectively (Figure 1B). The E484Q substitution in B.1.617.1 (B) only partially contributed to escape from neutralization (GMT 215) with a 2.5-fold reduction in neutralization compared to WT(D614G). Pseudoviruses with single L452R and T478K substitutions each conferred a similar fold change in resistance (1.3- and 1.5-fold, respectively) as B.1.617.2 (1.6-fold) compared to WT(D614G), although a 2.4-fold reduction was seen against the pseudoviruses with the dual L452R + T478K substitutions. This latter finding suggests that substitutions outside of the RBD may be modifying resistance to B.1.617.1 (B) in those infected individuals.

Sera from the group infected by variants that had the L452R substitution showed similar fold changes in neutralization titers as the group infected by WT(D614G) variants without the L452R except against B.1.617.1 (B) and AY.1 pseudoviruses. Fold changes in neutralization titers against B.1.617.1 (B) and AY.1 variants were 3.3 and 1.3, respectively, for the L452 group, compared to 5.2 and 2.5, respectively, for the WT(D614G) group (Figure 1B,C). The fold reduction of neutralization titers against variants containing substitutions at L452 position, including B.1.617.2, AY.1, B.1.617.1, C.37, and L452R RBD substitution mutant, compared to WT(D614G) also trended lower in the group infected by the L452R variant compared to the group infected by the WT(D614G) variant. These findings extend a prior study reporting that spike-binding titers in convalescent sera from unvaccinated persons were decreased 4- to 6-fold for B.1.617.2 when compared to B.1.1.7 and WT(D614G) [41]. The generally lower titers and small numbers of samples in the L452R group in our study may impact the fold changes. We also note that in our study the titers of the sera from WT(D614G)-infected individuals are generally higher than the neutralization titers of the sera from L452R-infected individuals, but the small number of samples prevents a meaningful comparison. Differences in titers may be due to the timing of collection of sera since infection, severity of infection, or other factors.

3.2. Neutralization of B.1.617 Variant Pseudoviruses by Vaccine-Elicited Sera

We next assessed the neutralization potency of mRNA vaccine-elicited sera against WT(D614G) and B.1.617 variant pseudoviruses. Sera from fourteen individuals who received two doses of Moderna mRNA-1273 vaccine and fifteen individuals who received two doses of Pfizer/BioNtech BNT162b2 vaccine were collected approximately two weeks after the second immunization. Each vaccine-elicited serum had high neutralization titers against WT(D614G) pseudoviruses, ranging between 578 and 3935 for Pfizer/BioNtech BNT162b2 and 651 and 5853 for Moderna mRNA-1273 (Figure 2A,B) (Pfizer/BioNtech BNT162b2 vs. Moderna mRNA-1273, $p = 0.1225$, Mann–Whitney test). The Moderna mRNA-1273 vaccine-elicited sera trended towards higher neutralization titers against most variants compared to Pfizer/BioNtech BNT162b2, possibly due to higher vaccine mRNA content and greater interval between priming and boosting for Moderna mRNA-1273 (4 weeks vs. 3 weeks for Pfizer/BioNtech BNT162b2) [42]. Compared to WT, a similar reduction in neutralization towards B.1.617.1, B.1.617.2, and AY.1 was noticed for

both Pfizer/BioNtech BNT162b2 and Moderna mRNA-1273 vaccine-elicited sera. The average neutralization potency of Pfizer/BioNtech BNT162b2 vaccine-elicited sera was 2–2.5-fold lower against B.1.617.1 pseudoviruses (GMT 642 for B.1.617.1 (A); GMT 519 for B.1.617.1 (B)) compared to WT(D614G) (GMT 1310) and 1.9–2.8-fold lower for B.1.617.2 pseudoviruses (GMT 693 for B.1.617.2; GMT 469 for AY.1 pseudovirus) compared to WT(D614G) (GMT1310) (Figure 2A). The average neutralization potency of Moderna mRNA-1273-elicited sera was 2–2.4-fold reduced against B.1.617.1 (GMT 1019 for B.1.617.1 (A); GMT 856 for B.1.617.1 (B)) compared to WT(D614G) (GMT2015) and 1.8–3.4-fold lower against B.1.617.2 pseudoviruses (GMT 1095 for B.1.617.2; GMT 597 for AY.1) (Figure 2B). Our findings agree with a recent study that showed 3.0-, 2.4-, and 4.1-fold reduction of Pfizer/BioNtech BNT162b2-elicited plasma neutralization, and 4.1-, 2.6-, and 9.5-fold reduction of Moderna mRNA-1273-elicited plasma neutralization for B.1.617.1, B.1.617.2, and AY.1 pseudoviruses, respectively, compared to WT(D614G) [38,39].

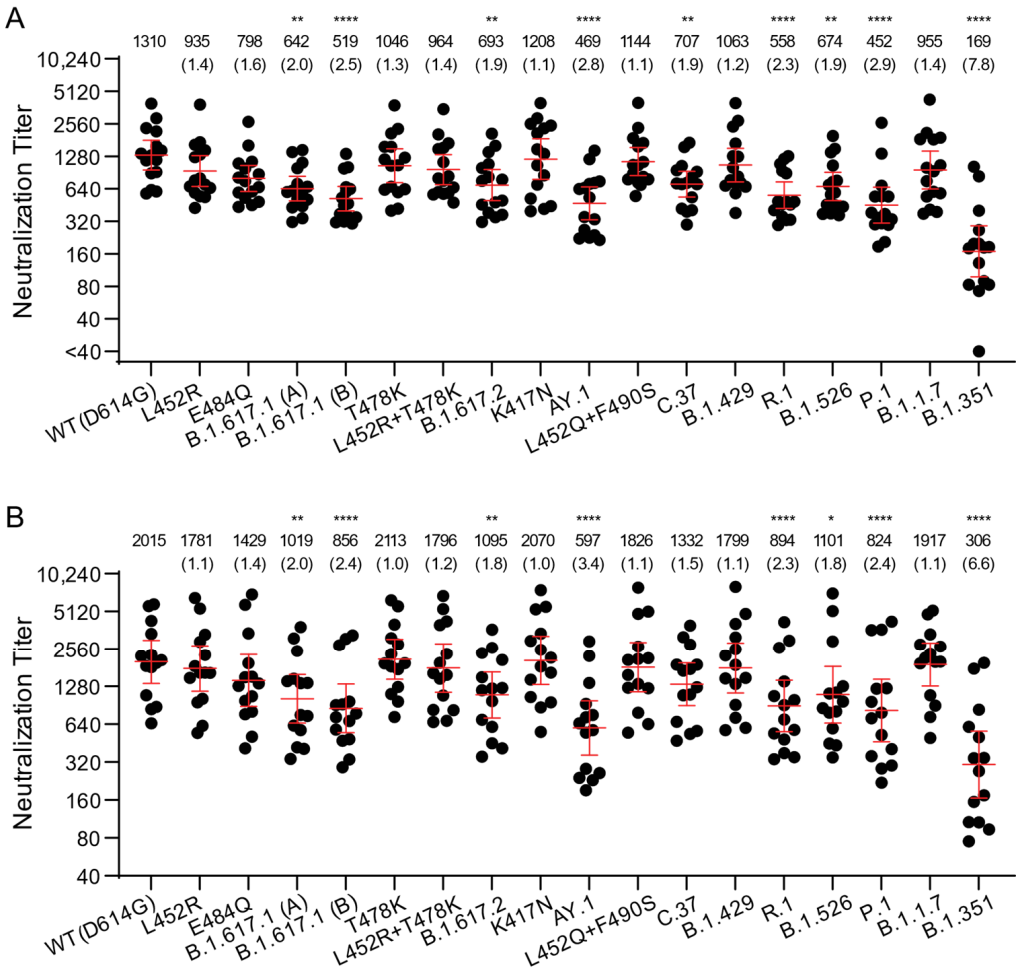

Figure 2. Neutralization of variant SARS-CoV-2 pseudoviruses by vaccine-elicited sera. The neutralization titers represented as 50% inhibitory concentrations (IC_{50}) against pseudoviruses bearing spike proteins from the indicated variants are plotted. (**A**) Neutralization titers of Pfizer/BioNtech BNT162b2 vaccination sera are presented. (**B**) Neutralization titers of Moderna mRNA-1273 vaccination sera are presented. Bars: geometric means of titers (GMT) with 95% CI. The numbers over each graph indicate the GMT. The numbers in parentheses are the ratios of WT(D614G) GMT/individual variant GMT. *p* values were calculated by one-way analysis of variance (ANOVA) with Dunnett's multiple comparisons tests (variants compared to WT(D614G)). Titers measuring below the lowest serum dilution of 1:40 were treated as 20 for statistical analysis. All neutralization titers were $\log_2$ transformed before test. *: $p \leq 0.05$; **: $p \leq 0.01$; ****: $p \leq 0.0001$.

We also investigated the contribution of individual RBD substitutions of B.1.617.1 (L452R, E484Q) and B.1.617.2/AY.1 (K417N, L452R, T478K) on the D614G background. Titers against L452R (GMT 935 for Pfizer and 1781 for Moderna) and E484Q (GMT 798 for Pfizer and 1429 for Moderna) alone trended slightly lower. Likewise, titers against K417N (GMT 1208 for Pfizer and 2070 for Moderna) and T478K (GMT 1046 for Pfizer and 2113 for Moderna) alone or in L452R + T478K combination (GMT 964 for Pfizer and 1796 for Moderna) remained comparable to GMTs of WT(D614G) (Figure 2 and Supplementary Figure S2).

Similarly, GMTs against B.1.1.7 (955 for Pfizer and 1917 for Moderna) and B.1.429 variant with the L452R substitution (1063 for Pfizer and 1799 for Moderna) were comparable to those against WT(D614G). Consistent with previous observations, the B.1.351 variant (GMT 169 for Pfizer and 306 for Moderna) displayed ~7-fold lower titers compared to WT(D614G), whereas C.37, P.1, R.1, and B.1.526 variants displayed modestly reduced titers that are similar to the titers against B.1.617 pseudoviruses (GMT 452–707 for Pfizer and GMT 824–1332 for Moderna). Overall, the trends in neutralization titers for the vaccine-elicited sera against a large panel of variant pseudoviruses were similar to those for convalescent sera, though the GMTs were approximately 3- to 5-fold higher for vaccine-elicited sera.

A prior study showed that convalescent sera and vaccine-elicited antibody neutralization titers against pseudoviruses bearing spikes containing L452R-E484Q-P681R substitutions displayed 2–5-fold reduction, compared to the neutralization titers against WT(D614G) pseudoviruses [25]. In this study, depending upon the infecting variant, convalescent sera displayed a modest 2–4-fold reduction in neutralization titers for B.1.617.1 compared to WT(D614G), while the vaccine-elicited sera displayed only 2.1-fold reduction. Our findings using B.1.617.1 pseudoviruses with the full complement of spike substitutions rather than just the L452R-E484Q-P681R spike substitutions confirm and extend the prior findings [25]. Finally, the 1.8–3.4-fold reduction in neutralization in the vaccination group against B.1.617.2 pseudoviruses seen in our study and others suggests that the two-dose mRNA vaccines could significantly contribute to protection against both Kappa and Delta variants [17,18,38,41,43].

3.3. Antigenic Cartography

We used antigenic cartography to compare the relative difference in neutralization of distinct variants, exploiting heterogeneity in individual antibody responses to identify antigenic differences among strains. Antigenic map dimensionality was tested in 1–5 dimensions using cross-validation. The 3D maps had only slightly greater predictive power compared to the 2D maps; both the 2D and 3D maps performed much better than 1D (Supplementary Table S1). The 2D antigenic maps are presented for convalescent infection sera (Figure 3A) and vaccine sera (Figure 3B). To evaluate reproducibility in positioning of antigens on the map, we created bootstrap confidence intervals in which n = 10,000 antigenic maps were made by resampling sera with replacement (bottom panels in Figure 3A,B). Antigenic maps are also shown in 3D (Supplementary Figure S3). Maps made with convalescent sera only from infection by WT(D614G) or only from infection by strains containing L452R mutation were not sufficiently robust for antigen positioning.

On the convalescent sera antigenic map, most of the pseudoviruses clustered close to the WT(D614G) pseudovirus and the WT(D614G) sera and L452R sera, including K417N, L452R, T478K, L452Q + F490S, and B.1.429 (0.25 to 0.72 antigenic units (AU) from WT (Table 3). B.1.617.2, C.37, and AY.1 clustered below WT(D614G) and slightly further away (1.14–1.60 AU), while L452R + T478K was also further away, but in the opposite direction (1.20 AU). However, in the bootstrap confidence interval 2D map and 3D map, L452R + T478K and AY.1 had distinct positions, clustering together with B.1.617.2 and C.37 in the 3D map and together but with T478K on the bootstrap 2D map. On all maps, B.1.351 was the most distinct from WT(D614G) (4.90 AU), followed by B.1.617.1 (2.78 AU), positioned between B.1.617.2 and B.1.351, and E484Q (1.77 AU), which was between WT(D614G) and B.1.351. These findings suggest that the full set of RBD substitutions

in combination with substitutions outside the RBD contributes to antigenic difference of B.1.617.1, B.1.617.2, C.37, and B.1.351, while RBD substitutions alone in the WT(D614G) background do not reflect what is observed for each respective variant.

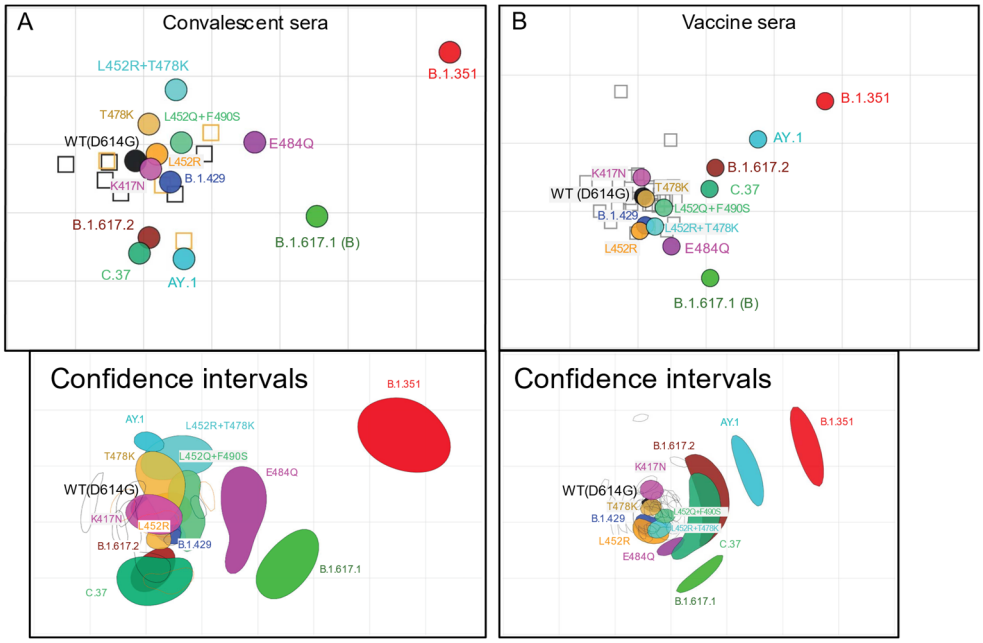

Figure 3. Antigenic maps of SARS-CoV-2 variants made using antigenic cartography. Two-dimensional antigenic maps were made using neutralizing antibody titers from convalescent sera (**A**) and vaccine sera (**B**). Convalescent sera map (**A**) includes sera from the group of WT(D614G)-infected individuals and the group of individuals infected with strains containing L452R mutation. Vaccine sera map (**B**) includes sera from individuals vaccinated with Pfizer/BioNtech BNT162b2 and individuals vaccinated with Moderna mRNA-1273 vaccine. Sera are shown as open squares and pseudoviruses are shown as colored circles, labeled by strain name. Each grid-square corresponds to a two-fold dilution in the pseudovirus neutralization assay. Antigenic distance is interpretable in any direction. Antigenic maps shown with 70% bootstrap confidence intervals to convey uncertainty in positioning of antigens and sera are shown in the bottom panel of (**A**,**B**). Two-dimensional antigenic maps with confidence intervals for the position of each antigen and antiserum were made from 10,000 bootstrap resampled maps, each made by bootstrap sampling of antisera.

Table 3. Antigenic units (AU) from WT(614G) on 2D antigenic maps.

Pseudovirus	Convalescent Sera	Vaccine Sera
WT(D614G)	0.00	0.00
K417N	0.25	0.28
L452R	0.33	0.51
T478K	0.57	0.05
B.1.429	0.60	0.43
L452Q-F490S	0.72	0.35
B.1.617.2	1.14	1.14
L452R-T478K	1.20	0.48
C.37	1.35	0.98
AY.1	1.60	1.89
E484Q	1.77	0.84
B.1.617.1	2.78	1.55
B.1.351	4.88	3.02

The antigenic map of the same SARS-CoV-2 variant pseudoviruses for vaccine-elicited sera showed similar patterns to the convalescent sera map but with some notable differ-

ences. Again, pseudoviruses K417N, L452R, T478K, L452Q + F490S, and B.1.429 were close to WT(D614G) (0.05–0.51 AU). However, E484Q and C.37 were both closer to WT(D614G) but were poorly coordinated and extended in elongated shapes around WT(D614G). B.1.617.1 was also slightly closer to WT(D614G) at 1.55 AU and was positioned adjacent to the other variants. Unexpectedly, AY.1 was between B.1.617.2 and B.1.351 and was further away from WT(D614G) (1.89 AU) than in the convalescent sera map (1.60 AU), being positioned only slightly closer to WT(D614G) than B.1.351 was from WT(D614G) (3.02 AU). These antigenic maps reinforce what was observed in terms of neutralizing antibody titers. Compared to the convalescent sera map, there was a larger antigenic difference between AY.1 and WT(D614G) on the vaccine-elicited sera map.

Notably, given that the vaccine-elicited sera had much higher titers than convalescent sera across variants, the titers against AY.1 were still higher in vaccinated individuals, meaning the antigenic difference may not translate into loss of vaccine protection. Furthermore, vaccine-elicited sera saw a smaller difference between B.1.351 and WT(D614G) than the convalescent sera, which may have aligned AY.1 and B.1.351 closer together. Overall, while these antigenic maps provide meaningful information on the relative positions of antigens, they are limited by the sera being so tightly clustered. Future antigenic maps with sera against distinct variants would enable more accurate evaluation of antigenic variation among the variants.

3.4. Spike RBD Substitutions in B.1.617 Variants Affect Sensitivity to Therapeutic Antibodies

We next evaluated 23 clinical-stage therapeutic neutralizing antibodies for potency against the B.1.617 variants. These antibodies were evaluated as part of the U.S. Government COVID-19 response effort to inform the clinical testing and use of these antibodies [19]. Due to an agreement with the manufacturers who provided the antibodies, only blind codes are used to identify the antibodies. Amongst the therapeutic antibodies tested were thirteen nAbs, six cnAbs, and four pAbs.

B.1.617.1 pseudoviruses displayed complete resistance (>50-fold) to five nAbs (C, D, E, F, and G) and partial resistance (10–50-fold) to one nAb (H) (Figure 4A and Supplementary Figure S4). The E484Q substitution alone conferred complete resistance (>50-fold) to three nAbs (E, F, and G), and partial resistance to one nAb (C) as previously described [19,44]. The L452R substitution also conferred complete resistance to four nAbs (C, D, E, and H), as previously described [19]. The L452R is centrally located in the receptor-binding site and is a known resistance substitution for several mAbs [23,26]. None of the cnAbs and pnAbs tested showed the loss of neutralization potency against L452R, E484Q, and B.1.617.1 (Supplementary Figure S4). Overall, these findings show that the E484Q and L452R substitutions fully account for the resistance of B.1.617.1 against these nAbs, while 17 of 23 tested therapeutic antibodies retained neutralization potency against B.1.617.1 (Supplementary Figure S4).

B.1.617.2 pseudoviruses displayed complete resistance (>50-fold) to three nAbs (C, D, and E) and partial resistance (10–50-fold) to one nAb (H) (Figure 3B). The L452R substitution alone is responsible for the resistance of these nAbs (C, D, E, and H) as pseudoviruses bearing L452R alone or in combination with T478K (L452R + T478K) displayed identical patterns of resistance as B.1.617.2 pseudoviruses. AY.1 pseudoviruses displayed similar resistance to the nAbs as B.1.617.2 pseudoviruses, except for complete resistance to one additional nAb (N) due to the K417N RBD substitution and one cnAb (S) (Figure 4C).

3.5. B.1.617 Pseudovirus Infectivity and Spike Protein Processing

Prior reports indicated increased infectivity of pseudoviruses containing the L452R substitution in spike in 293T-ACE2.TMPRSS2 cells due to L452R conferring enhanced RBD affinity to ACE2 [24,27]. We therefore investigated the impact of the B.1.617 spike substitutions on pseudovirus infectivity and found that B.1617.1, B.1.617.2, and AY.1 pseudoviruses, as well as pseudoviruses with single RBD L452R, T478K, and E484Q substitutions, displayed similar infectivity to WT(D614G) (Supplementary Figure S5).

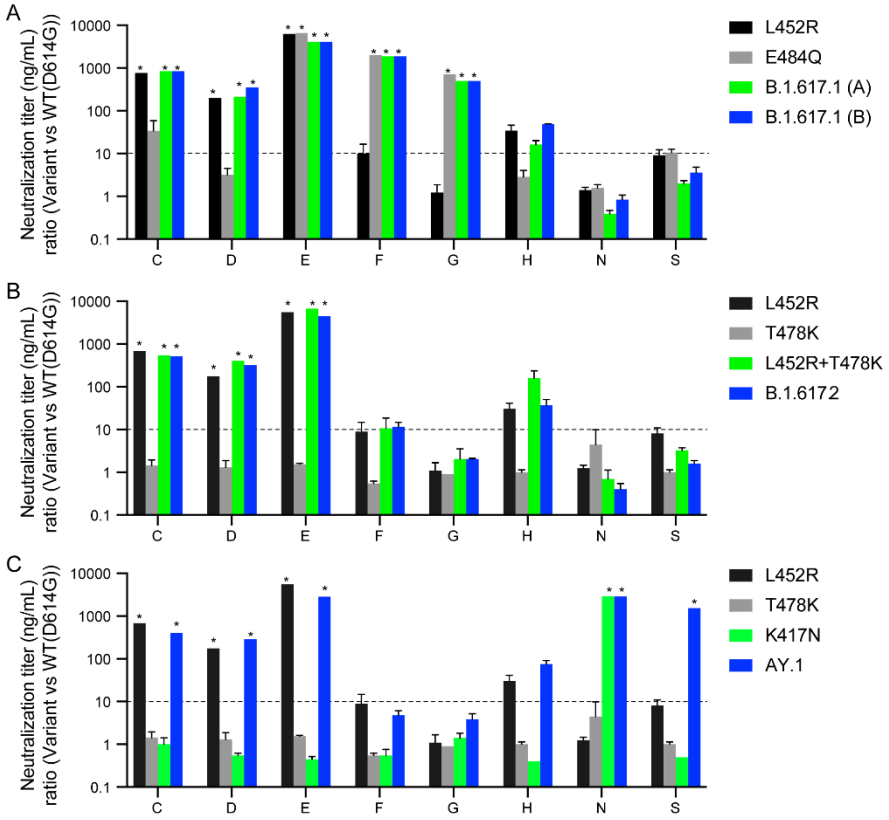

Figure 4. Neutralization of variant SARS-CoV-2 pseudoviruses by therapeutic antibodies. The antibody panel, consisting of 15 single neutralizing Abs (nAbs A–R), six combination Abs (S–X), and two polyclonal Abs (III–IV), were tested against SARS-CoV-2 pseudoviruses bearing the indicated spike proteins. Only those that displayed significant neutralization resistance compared to WT(D614G) are shown (Refer to Supplementary Figure S4 for remaining antibodies). Antibodies are blinded according to an agreement with the manufacturers. The neutralization titer (IC_{50}) ratios of the B.1.617.1 variants (**A**), B.1.617.2 variant (**B**), and AY.1 variant (**C**) relative to WT(D614G) are plotted. The dotted lines represent the neutralization titer ratio of 10. *: complete resistance at the highest concentration tested (>50-fold change of IC_{50}).

Previous studies demonstrated that L452R, and N501Y substitutions in RBD enhanced spike protein affinity to ACE2, which may have contributed to greater transmissibility of B.1.1.7, B.1.351, P.1, and B.1.427/429 variants [45–47]. To investigate whether the B.1.617 variants have an increased binding for ACE2, we measured the neutralization potency of human soluble ACE2 (sACE2) protein against the variants. We found that the 50% inhibitory concentrations (IC_{50}) of sACE2 against B.1.617.2 (IC_{50}: 0.68 µg/mL; $p < 0.01$) was 4.2-fold lower, compared to WT(D614G) (IC_{50}: 2.88 µg/mL) (Table 4 and Supplementary Figure S6). In agreement with greater ACE2 affinity of L452R RBD compared to WT RBD as reported by others using surface plasmon resonance [27,48], pseudoviruses containing L452R (IC_{50}:1.19 µg/mL; $p < 0.05$) and L452R + T478K (IC_{50}:1.23 µg/mL; $p < 0.001$) displayed 2.4- and 2.3-fold higher sensitivity to inhibition by sACE2. However, pseudoviruses with only spike RBD substitutions (T478K, E484Q), as well as the B.1.617.1 (IC_{50}:2.03 µg/mL) and AY.1 (IC_{50}:1.97 µg/mL) spikes, displayed comparable IC_{50} to WT(D614G) (0.5–1.5-fold change) (Table 4 and Supplementary Figure S6). These findings suggest enhanced binding of Delta spike protein to the ACE2 receptor, which may potentially contribute to greater infectivity and replication in ACE2-positive target cells.

Table 4. Neutralization of B.1.617 pseudoviruses by soluble ACE2.

Pseudovirus	IC_{50} (μg/mL)	Fold Change (vs. WT(D614G))	*p* Value (vs. WT(D614G))
WT(D614G)	2.880	1.00	
B.1.617.1 (B)	2.028	1.420	<0.01
B.1.617.2	0.681	4.228	<0.01
AY.1	1.966	1.465	n.s.
L452R	1.189	2.422	<0.05
T478K	4.266	0.675	n.s.
L452R + T478K	1.228	2.345	<0.001
E484Q	5.568	0.517	n.s.

p values were calculated by one-way analysis of variance (ANOVA) with Dunnett's multiple comparisons tests (variants vs. WT(D614G)). n.s.: not significant.

Since P681H enhanced proteolytic processing of B.1.1.7 spike [29,49], we next evaluated spike proteolytic processing of B.1.617 pseudovirus variants carrying the P681R substitution. The B.1.617 variant pseudoviruses displayed efficient proteolytic processing of spike compared to Wuhan-Hu-1 (D614) and WT(D614G) as observed by the S1/S ratio (Figure 5A). We further evaluated the effect of P681R substitution on furin cleavage of SARS-CoV-2 by introducing this substitution in Wuhan-Hu-1 (D614) and WT(D614G) spike backgrounds. For all pseudoviruses bearing the P681R spike substitution, including B.1.617.1, B.1.617.2, Wuhan-Hu-1 + P681R, and P681R (+D614G), spike cleavage as determined by higher cleaved S1 subunit to total S (S1 + S) ratios was enhanced compared to the respective original pseudoviruses (Figure 5A). B.1.1.7 and WT(D614G) pseudoviruses bearing P681H also displayed enhanced spike cleavage (Figure 5A), consistent with previous reports [29,50]. B.1.429 pseudoviruses that lack P681R or P681H substitutions near the furin cleavage site displayed inefficient spike cleavage, whereas the furin cleavage site (ΔPRRA)-deleted spike lacked cleavage. Our findings agree with several studies reporting enhanced furin cleavage efficiency of B.1.1.7 and B.1.617 spikes bearing P681H and P681R substitutions, respectively [49–52].

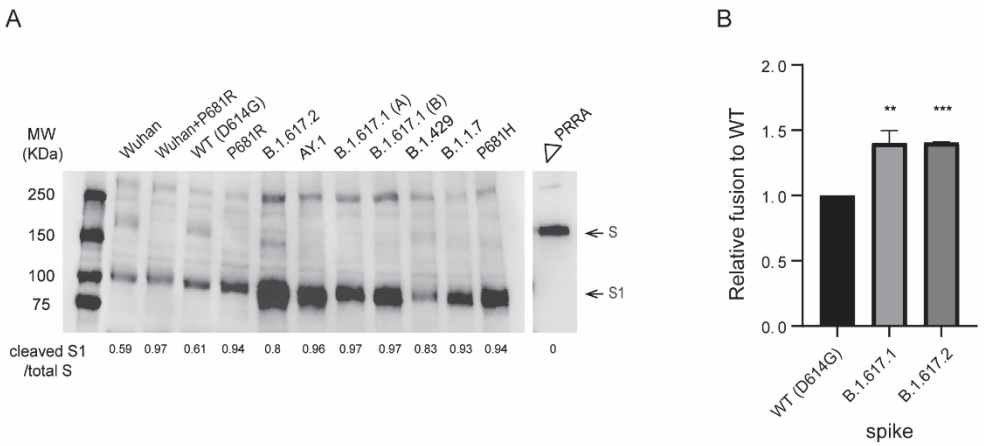

Figure 5. Proteolytic processing and fusogenic activity of B.1.617 variant spike proteins. (**A**) Western blot analysis of SARS-CoV-2 spike content of pseudoviruses. S/S1 was detected using a rabbit antibody against the SARS-CoV-2 S1 region. The image was a representation of three independent Western blots. (**B**) Spikes-induced cell-cell fusion quantified by β-galactosidase complementation assay. Y-axis indicates the relative β-galactosidase activity in variant spikes induced cell-cell fusion compared to WT(D614G) spike at 24 h post co-culturing of spike-transfected 293T-ω cells and α-subunit-transfected 293T.ACE2.TMPRSS2 cells. X-axis indicates transfected spike in 293T-ω cells. Bars: mean +/− SD of four independent experiments. *p* values were calculated by one-way analysis of variance (ANOVA) with Dunnett's multiple comparisons tests (variants vs. WT(D614G)). **: $p \leq 0.01$, ***: $p \leq 0.001$.

To gain further insight into the furin processing efficiency at the S1/S2 site of the B.1.617 S, we undertook a bioinformatic approach utilizing the PiTou and ProP furin cleavage prediction tools, comparing B.1.617 to the Wuhan-Hu-1 (D614) prototype spike and B.1.1.7 spike, as well as spike proteins of several lineage-specific mammalian and animal CoVs. The PiTou algorithm combines a hidden Markov model and knowledge-based cumulative probability score functions for the functional characterization of a 20 amino acid cleavage motif from P14 to P6′ for furin binding and cleavage, whereas ProP predicts furin cleavage sites based on experimental data-derived networks [53,54]. Both algorithms predicted a greater increase in the furin cleavage for B.1.617 lineage variants (PiTou: 12.4; Prop: 0.698) compared to Wuhan-Hu-1 (PiTou: 9.19; Prop: 0.62) and B.1.1.7 (PiTou: 9.9; Prop: 0.7) (Table 5) [54]. As expected, proteins not containing furin cleavage site displayed relatively lower scores while much higher scores were shown for the proteins containing furin cleavage site [55,56].

Table 5. Prediction scores of furin cleavage at S1/S2 junction in coronavirus spikes.

	S1/S2 Sequence	Furin PiTou Score	Furin Prop Score
Alphacoronavirus			
HCoV-NL63	564-GICADGSLIPVRPR | NSSDNG-583	−5.46642	0.105
HCoV-229E	748-GVCADGSIIAVQPR | NVSYDS-767	−5.4747	0.152
Betacoronavirus			
Lineage A			
HCoV-HKU1	760-YNSPSSSSSRRKRR | SISASY-779	14.6348	0.918
HCoV-OC43	763-GYCVDYFKNRRSRR | AITTGY-782	10.0989	0.736
Lineage B			
SARS-CoV	654-AGICASYHTVSLLR | STSQKS-757	−5.167	0.123
SARS-CoV-2 (Wuhan Hu-1)	672-ASYQTQTNSPRRAR | SVASQS-691	9.19633	0.62
SARS-CoV-2 (B.1.1.7)	672-ASYQTQTNSHRRAR | SVASQS-691	9.90746	0.704
SARS-CoV-2 (B.1.617)	672-ASYQTQTNSRRRAR | SVASQS-692	12.4069	0.698
Bat-CoV RaTG13	668-AGICASYQTQTNSR | SVASQS-687	−4.672	0.151
Bat-CoV ZC45	645-AGICASYHTASILR | STSQKA-664	−5.333	0.153
Bat-CoV ZXC21	645-AGICASYHTASILR | STGQKA-663	−5.333	0.17
Lineage C			
MERS-CoV	654-AGICASYHTVSLLR | STSQKS-673	−5.12695	0.563
Bat-CoV HKU4	736-GQSLCAVPPVSTFR | SYSASQ-755	-5.14	0.229
Bat-CoV HKU5	732-LCAIPPTTSSRVRR | ATSGAS-751	10.259	0.822
Bat-CoV PML	732-LCAIPPNTNLRSGR | STFGLG-751	2.175	0.572
Deltacoronavirus			
Avian infectious bronchitis virus	538-FYIKLTNGSRRFRR | SISSNV-557	11.375	0.848
Influenza A			
H5N1 HPAI (A/Chicken/Hong Kong/822.1/2001)	322-LRNTPQRERRRKKR | GLFGAI-341	13.59	0.808
H1N1 (A/California/04/pdm09)	344-LATGLRNIPSIQSR | GLFGAI-363	−4.72999	0.207
H3N2 (A/Wisconsin/67/2005)	345-LATGMRNVPEKQTR | GIFGAI-364	−5.10067	0.165

While SARS-CoV-2 S1/S2 P−R−R−A−R furin cleavage site conforms to a minimal furin recognition motif, R−X−X−R, the presence of H/R instead of P increases the total number of basic residues to four. This presence of basic residue H/R results in additional electrostatic and intramolecular hydrogen bonding to gain substrate turnover [57]. In fact, this basic residue is represented in several viral and cellular proteins [57,58]. While the cleavage is not necessary to enhance pseudovirus infectivity, the furin cleavage of spike has been shown to be necessary for the virus transmission as demonstrated in a ferret model [59]. The P681H substitution in B.1.1.7 variants has been associated with enhanced virus transmissibility whereas the P681R substitution in B.1.617 variants has been associated with enhanced pathogenicity in a hamster model and transmissibility [29,59–61]. Further investigations of the role of P681H/R substitutions for virus transmissibility and cell-to-cell spread in in vivo animal models are needed. Furthermore, continued surveillance is necessary as several independent lineages have recently emerged containing

additional substitutions proximal to S1/S2 cleavage junction, such as the B.1.2 and B.1.525 with Q677H, C.37 and B.1.617.2 with Q675H, and C.1.2 with N679K substitutions [62,63]. On the other hand, functions of furin cleavage site substitutions in host cell attachment and antigenicity cannot be excluded since amino acids N^{679}- R^{685} and E^{661}- R^{685} have been reported to have host neuropilin-1 attachment [64] and staphylococcus-enterotoxin-B-like super-antigenic functions [65].

Furin cleavage score analysis of CoV S1/S2 cleavage sites. CoV spike and influenza hemagglutinin (HA) sequences were analyzed using the ProP 1.0 and PiTou 3.0 furin prediction algorithms, generating a score with bold numbers indicating predicted furin cleavage. "|" denotes the position of the furin cleavage site. Sequences corresponding to the S1/S2 region of NL63 (APF29063.1), 229E (ABB90529.1), SARS-CoV-2 (QHD43416.1), SARS-CoV (AAT74874.1), MERS-CoV (AFS88936.1), HCoV-HKU1 (AAT98580.1), HCoV-OC43 (APU51936) Bat-SL-CoVZC45 (AVP78031.1) BatCoV-HKU4 (YP_001039953.1), Influenza A/Chicken/Hong Kong/822.1/01/H5N1 HA (AF509026.2), Influenza A virus HA (A/Wisconsin/67/2005(H3N2) (ACF54576.1), infectious bronchitis virus (QIV13719.1), CoV-HKU9 (YP_001039971), BatCoV-PML (AGY29650), BatCoV-HKU5 (YP_001039962.1), Bat-CoV RaTG13 (QHR63300.2), and Bat-SL-CoVZXC21 (AVP78042.1) were obtained from GenBank. Sequences corresponding to the S1/S2 region of SARS-CoV-2 B.1.1.7 (EPI_ISL_1374509), B.1.617.1 (EPI_ISL_1841346), B.1.617.2 (EPI_ISL_2229775), B.1.617.3 (EPI_ISL_2157058), Bat CoV RmYN02 (EPI_ISL_412977), as well as HA of Influenza A virus (A/California/04/pdm09 (H1N1)) (EPI1859607) were obtained from GISAID.

3.6. B.1.617 Spike-Mediated Cell-Cell Fusion

To quantify whether higher ACE2 binding and furin cleavage of B.1.617.2 spike augments fusion between virus and/or cell membranes, we performed cell-cell fusion assays by complementing β-galactosidase subunits in spike-transfected effector cells and 293T-ACE2.TMPRSS2 target cells. Compared to WT(D614G), both B.1.617.1 and B.1.617.2 spikes induced significantly higher cell-cell fusion activity when controlled for spike cell surface expression (4000 MFI of spike protein on cell surface) (Figure 5B). Our findings extend previous studies indicating that the P681R substitution increases spike proteolytic cleavage and facilitates cell-cell fusion [41,50,66,67]. Our findings also suggest that fusogenic potential of spike proteins may be influenced by both ACE2 binding affinity as well as proteolytic cleavage of spike.

4. Conclusions

Here we show that pseudoviruses bearing B.1.617.1 spike with L452R and E484Q substitutions, and B.1.617.2 spike with K417N, L452R and T478K substitutions, have modestly reduced susceptibility to neutralization by Pfizer/BioNtech BNT162b2 or Moderna mRNA-1273 vaccine-elicited sera and convalescent sera compared to pseudoviruses bearing WT(D614G) spike. The individual L452R, T478K, E484Q, and dual L452R + T478K substitutions accounted for most but not all of the reduction in neutralization potency of the sera, suggesting contributions from substitutions in the NTD/CTD. Neutralization titers, as well as antigenic maps, indicated that the full set of RBD substitutions in combination with substitutions outside the RBD contributes to antigenic differences of B.1.617.1, B.1.617.2, and C.37 variants. Antigenic distances between the variants also tended to be more spaced apart in the map generated by the convalescent sera compared to the vaccine-elicited sera. Limitations in our study include the small number of sera samples in the convalescent and vaccine cohorts. Potential differences in COVID-19 severity in the convalescent sera cohort and time of sera collection could also affect neutralization titers. Nonetheless, most sera from convalesced and vaccinated individuals neutralized the B.1.617.1, B.1.617.2, and AY.1 variants. Furthermore, 17 of 23 therapeutic neutralizing antibodies retained complete neutralization against B.1.617 variants. Resistance to the remaining therapeutic neutralizing antibodies is due to RBD substitutions, K417N, L452R, and E484Q, but not T478K. These findings suggest that the two-dose immunization with current mRNA vaccines

will likely induce protective immunity against the tested B.1.617 variants. However, as B.1.617.2 variants continue to evolve, it will be important to continue to monitor how new substitutions in spike impact their resistance to therapeutic neutralizing antibodies and vaccine efficacy.

Supplementary Materials: The following are available online at https://www.mdpi.com/article/10.3390/v13122485/s1: Figure S1: SARS-CoV-2 Wuhan-Hu-1 spike gene open reading frame comparison; Figure S2. Neutralization of variant SARS-CoV-2 pseudoviruses by vaccination sera; Figure S3. 3D antigenic maps of SARS-CoV-2 variants made using antigenic cartography; Figure S4. Neutralization of variant SARS-CoV-2 pseudoviruses by therapeutic antibodies; Figure S5. Infectivity of pseudoviruses with variants spikes; Figure S6. Neutralization of B.1.617 variant pseudoviruses by soluble ACE2; Table S1. Dimensionality testing of Antigenic Cartography maps.

Author Contributions: Conceptualization, S.N.N., K.J.E., C.D.W., A.E.E., and W.W.; methodology, S.N.N., C.D.W., W.W., R.V., S.L., and R.W.; software, F.E., L.C.K., L.B., K.J.E., and W.W.; validation, R.V., S.L., C.D.W., and W.W.; formal analysis, S.N.N., R.V., S.L., L.B., K.J.E., F.E., L.C.K., C.D.W., and W.W.; investigation, S.N.N., W.W., R.V., S.L., and R.W.; resources, C.D.W., L.C.K., and A.E.E.; data curation, R.V., L.B., S.L., F.E., and W.W.; writing—original draft preparation, S.N.N. and W.W.; writing—review and editing, C.D.W., L.C.K., A.E.E., and K.J.E.; visualization, S.L., S.N.N., F.E., L.C.K., and W.W.; supervision, C.D.W.; project administration, C.D.W.; funding acquisition, A.E.E. All authors have read and agreed to the published version of the manuscript.

Funding: This project was funded in part by the National Institute of Allergy and Infectious Diseases through an interagency agreement (AAI21013-001-00000) with Center for Biologics Evaluation and Research, US Food and Drug Administration (CBER/FDA), as part of the US Government COVID-19 response efforts, by FDA institutional research funds, and by the Intramural Research Program of the National Institute of Allergy and Infectious Diseases to F.E. and L.C.K.

Institutional Review Board Statement: The use of de-identified sera and neutralizing antibodies in this study was approved by the U.S. Food and Drug Administration Research in Human Subjects Committee. Vaccine-elicited sera were collected at the U.S. Food and Drug Administration with written consent under an approved Institutional Review Board (IRB) protocol (FDA IRB Study # 2021-CBER-045).

Informed Consent Statement: Informed consent was obtained from all subjects involved in the study.

Acknowledgments: The authors would like to thank Hongquan Wan (FDA), and Hailun Ma (FDA) for the critical review of the manuscript.

Conflicts of Interest: The authors declare no conflict of interest.

References

1. Baden, L.R.; El Sahly, H.M.; Essink, B.; Kotloff, K.; Frey, S.; Novak, R.; Diemert, D.; Spector, S.A.; Rouphael, N.; Creech, C.B.; et al. Efficacy and Safety of the mRNA-1273 SARS-CoV-2 Vaccine. *N. Engl. J. Med.* **2021**, *384*, 403–416. [CrossRef]
2. Sadoff, J.; Le Gars, M.; Shukarev, G.; Heerwegh, D.; Truyers, C.; de Groot, A.M.; Stoop, J.; Tete, S.; Van Damme, W.; Leroux-Roels, I.; et al. Interim Results of a Phase 1–2a Trial of Ad26.COV2.S Covid-19 Vaccine. *N. Engl. J. Med.* **2021**, *384*, 1824–1835. [CrossRef] [PubMed]
3. Madhi, S.A.; Baillie, V.; Cutland, C.L.; Voysey, M.; Koen, A.L.; Fairlie, L.; Padayachee, S.D.; Dheda, K.; Barnabas, S.L.; Bhorat, Q.E.; et al. Efficacy of the ChAdOx1 nCoV-19 Covid-19 Vaccine against the B.1.351 Variant. *N. Engl. J. Med.* **2021**, *384*, 1885–1898. [CrossRef]
4. Walls, A.C.; Park, Y.-J.; Tortorici, M.A.; Wall, A.; McGuire, A.T.; Veesler, D. Structure, Function, and Antigenicity of the SARS-CoV-2 Spike Glycoprotein. *Cell* **2020**, *181*, 281–292.e6. [CrossRef]
5. Hoffmann, M.; Kleine-Weber, H.; Krüger, N.; Mueller, M.A.; Drosten, C.; Pöhlmann, S. The novel coronavirus 2019 (2019-nCoV) uses the SARS-coronavirus receptor ACE2 and the cellular protease TMPRSS2 for entry into target cells. *bioRxiv* **2020**. [CrossRef]
6. Wrapp, D.; Wang, N.; Corbett, K.S.; Goldsmith, J.A.; Hsieh, C.-L.; Abiona, O.; Graham, B.S.; McLellan, J.S. Cryo-EM structure of the 2019-nCoV spike in the prefusion conformation. *Science* **2020**, *367*, 1260–1263. [CrossRef] [PubMed]
7. Shang, J.; Wan, Y.; Luo, C.; Ye, G.; Geng, Q.; Auerbach, A.; Li, F. Cell entry mechanisms of SARS-CoV-2. *Proc. Natl. Acad. Sci. USA* **2020**, *117*, 11727–11734. [CrossRef]
8. Korber, B.; Fischer, W.M.; Gnanakaran, S.; Yoon, H.; Theiler, J.; Abfalterer, W.; Hengartner, N.; Giorgi, E.E.; Bhattacharya, T.; Foley, B.; et al. Tracking Changes in SARS-CoV-2 Spike: Evidence that D614G Increases Infectivity of the COVID-19 Virus. *Cell* **2020**, *182*, 812–827.e19. [CrossRef] [PubMed]

9. Plante, J.A.; Liu, Y.; Liu, J.; Xia, H.; Johnson, B.A.; Lokugamage, K.G.; Zhang, X.; Muruato, A.E.; Zou, J.; Fontes-Garfias, C.R.; et al. Spike mutation D614G alters SARS-CoV-2 fitness. *Nature* **2021**, *592*, 116–121. [CrossRef]
10. Yurkovetskiy, L.; Wang, X.; Pascal, K.E.; Tomkins-Tinch, C.; Nyalile, T.P.; Wang, Y.; Baum, A.; Diehl, W.E.; Dauphin, A.; Carbone, C.; et al. Structural and Functional Analysis of the D614G SARS-CoV-2 Spike Protein Variant. *Cell* **2020**, *183*, 739–751.e8. [CrossRef] [PubMed]
11. Zhou, B.; Thao, T.T.N.; Hoffmann, D.; Taddeo, A.; Ebert, N.; Labroussaa, F.; Pohlmann, A.; King, J.; Steiner, S.; Kelly, J.N.; et al. SARS-CoV-2 spike D614G change enhances replication and transmission. *Nature* **2021**, *592*, 122–127. [CrossRef]
12. Weissman, D.; Alameh, M.-G.; de Silva, T.; Collini, P.; Hornsby, H.; Brown, R.; LaBranche, C.C.; Edwards, R.J.; Sutherland, L.; Santra, S.; et al. D614G Spike Mutation Increases SARS CoV-2 Susceptibility to Neutralization. *Cell Host Microbe* **2021**, *29*, 23–31.e4. [CrossRef] [PubMed]
13. Greaney, A.J.; Starr, T.N.; Gilchuk, P.; Zost, S.J.; Binshtein, E.; Loes, A.N.; Hilton, S.K.; Huddleston, J.; Eguia, R.; Crawford, K.H.; et al. Complete Mapping of Mutations to the SARS-CoV-2 Spike Receptor-Binding Domain that Escape Antibody Recognition. *Cell Host Microbe* **2021**, *29*, 44–57.e9. [CrossRef]
14. Baum, A.; Fulton, B.O.; Wloga, E.; Copin, R.; Pascal, K.E.; Russo, V.; Giordano, S.; Lanza, K.; Negron, N.; Ni, M.; et al. Antibody cocktail to SARS-CoV-2 spike protein prevents rapid mutational escape seen with individual antibodies. *Science* **2020**, *369*, 1014–1018. [CrossRef]
15. Cele, S.; Africa, N.F.G.S.I.S.; Gazy, I.; Jackson, L.; Hwa, S.-H.; Tegally, H.; Lustig, G.; Giandhari, J.; Pillay, S.; Wilkinson, E.; et al. Escape of SARS-CoV-2 501Y.V2 from neutralization by convalescent plasma. *Nat. Cell Biol.* **2021**, *593*, 142–146. [CrossRef]
16. Zhou, D.; Dejnirattisai, W.; Supasa, P.; Liu, C.; Mentzer, A.J.; Ginn, H.M.; Zhao, Y.; Duyvesteyn, H.M.; Tuekprakhon, A.; Nutalai, R.; et al. Evidence of escape of SARS-CoV-2 variant B.1.351 from natural and vaccine-induced sera. *Cell* **2021**, *184*, 2348–2361.e6. [CrossRef]
17. Planas, D.; Bruel, T.; Grzelak, L.; Guivel-Benhassine, F.; Staropoli, I.; Porrot, F.; Planchais, C.; Buchrieser, J.; Rajah, M.M.; Bishop, E.; et al. Sensitivity of infectious SARS-CoV-2 B.1.1.7 and B.1.351 variants to neutralizing antibodies. *Nat. Med.* **2021**, *27*, 917–924. [CrossRef] [PubMed]
18. Wall, E.C.; Wu, M.; Harvey, R.; Kelly, G.; Warchal, S.; Sawyer, C.; Daniels, R.; Hobson, P.; Hatipoglu, E.; Ngai, Y.; et al. Neutralising antibody activity against SARS-CoV-2 VOCs B.1.617.2 and B.1.351 by BNT162b2 vaccination. *Lancet* **2021**, *397*, 2331–2333. [CrossRef]
19. Lusvarghi, S.; Wang, W.; Herrup, R.; Neerukonda, S.N.; Vassell, R.; Bentley, L.; Eakin, A.E.; Erlandson, K.J.; Weiss, C.D. Key substitutions in the spike protein of SARS-CoV-2 variants can predict resistance to monoclonal antibodies, but other substitutions can modify the effects. *J. Virol.* **2021**, 01110–01121. [CrossRef] [PubMed]
20. Wang, P.; Nair, M.S.; Liu, L.; Iketani, S.; Luo, Y.; Guo, Y.; Wang, M.; Yu, J.; Zhang, B.; Kwong, P.D.; et al. Antibody resistance of SARS-CoV-2 variants B.1.351 and B.1.1.7. *Nature* **2021**, *593*, 130–135. [CrossRef]
21. Chen, R.E.; Zhang, X.; Case, J.B.; Winkler, E.S.; Liu, Y.; VanBlargan, L.A.; Liu, J.; Errico, J.M.; Xie, X.; Suryadevara, N.; et al. Resistance of SARS-CoV-2 variants to neutralization by monoclonal and serum-derived polyclonal antibodies. *Nat. Med.* **2021**, *27*, 717–726. [CrossRef] [PubMed]
22. Tada, T.; Dcosta, B.M.; Samanovic, M.I.; Herati, R.S.; Cornelius, A.; Zhou, H.; Vaill, A.; Kazmierski, W.; Mulligan, M.J.; Landau, N.R. Convalescent-Phase Sera and Vaccine-Elicited Antibodies Largely Maintain Neutralizing Titer against Global SARS-CoV-2 Variant Spikes. *mBio* **2021**, *12*, e0069621. [CrossRef]
23. McCallum, M.; Bassi, J.; De Marco, A.; Chen, A.; Walls, A.C.; Di Iulio, J.; Tortorici, M.A.; Navarro, M.-J.; Silacci-Fregni, C.; Saliba, C.; et al. SARS-CoV-2 immune evasion by the B.1.427/B.1.429 variant of concern. *Science* **2021**, *373*, 648–654. [CrossRef]
24. Deng, X.; Garcia-Knight, M.A.; Khalid, M.M.; Servellita, V.; Wang, C.; Morris, M.K.; Sotomayor-González, A.; Glasner, D.R.; Reyes, K.R.; Gliwa, A.S.; et al. Transmission, infectivity, and neutralization of a spike L452R SARS-CoV-2 variant. *Cell* **2021**, *184*, 3426–3437.e8. [CrossRef]
25. Tada, T.; Zhou, H.; Dcosta, B.M.; Samanovic, M.I.; Mulligan, M.J.; Landau, N.R. Partial resistance of SARS-CoV-2 Delta variants to vaccine-elicited antibodies and convalescent sera. *iScience* **2021**, *24*, 103341. [CrossRef]
26. Starr, T.N.; Greaney, A.J.; Dingens, A.S.; Bloom, J.D. Complete map of SARS-CoV-2 RBD mutations that escape the monoclonal antibody LY-CoV555 and its cocktail with LY-CoV016. *Cell Rep. Med.* **2021**, *2*, 100255. [CrossRef]
27. Motozono, C.; Toyoda, M.; Zahradnik, J.; Saito, A.; Nasser, H.; Tan, T.S.; Ngare, I.; Kimura, I.; Uriu, K.; Kosugi, Y.; et al. SARS-CoV-2 spike L452R variant evades cellular immunity and increases infectivity. *Cell Host Microbe* **2021**, *29*, 1124–1136.e11. [CrossRef]
28. Zhang, L.; Jackson, C.B.; Mou, H.; Ojha, A.; Peng, H.; Quinlan, B.D.; Rangarajan, E.S.; Pan, A.; Vanderheiden, A.; Suthar, M.S.; et al. SARS-CoV-2 spike-protein D614G mutation increases virion spike density and infectivity. *Nat. Commun.* **2020**, *11*, 1–9. [CrossRef] [PubMed]
29. Lubinski, B.; Tang, T.; Daniel, S.; Jaimes, J.A.; Whittaker, G.R. Functional evaluation of proteolytic activation for the SARS-CoV-2 variant B.1.1.7: Role of the P681H mutation. *bioRxiv*. Available online: https://www.biorxiv.org/content/10.1101/2021.04.06.438731v2 (accessed on 29 October 2021). [CrossRef]
30. Starr, T.N.; Greaney, A.J.; Addetia, A.; Hannon, W.W.; Choudhary, M.C.; Dingens, A.S.; Li, J.Z.; Bloom, J.D. Prospective mapping of viral mutations that escape antibodies used to treat COVID-19. *Science* **2021**, *371*, 850–854. [CrossRef]

31. Naldini, L.; Blömer, U.; Gallay, P.; Ory, D.; Mulligan, R.; Gage, F.H.; Verma, I.M.; Trono, D. In Vivo Gene Delivery and Stable Transduction of Nondividing Cells by a Lentiviral Vector. *Science* **1996**, *272*, 263–267. [CrossRef] [PubMed]
32. Zufferey, R.; Nagy, D.; Mandel, R.J.; Naldini, L.; Trono, D. Multiply attenuated lentiviral vector achieves efficient gene delivery in vivo. *Nat. Biotechnol.* **1997**, *15*, 871–875. [CrossRef] [PubMed]
33. Neerukonda, S.N.; Vassell, R.; Herrup, R.; Liu, S.; Wang, T.; Takeda, K.; Yang, Y.; Lin, T.-L.; Wang, W.; Weiss, C.D. Establishment of a well-characterized SARS-CoV-2 lentiviral pseudovirus neutralization assay using 293T cells with stable expression of ACE2 and TMPRSS2. *PLoS ONE* **2021**, *16*, e0248348. [CrossRef]
34. Tada, T.; Fan, C.; Chen, J.S.; Kaur, R.; Stapleford, K.A.; Gristick, H.; Dcosta, B.M.; Wilen, C.B.; Nimigean, C.M.; Landau, N.R. An ACE2 Microbody Containing a Single Immunoglobulin Fc Domain Is a Potent Inhibitor of SARS-CoV-2. *Cell Rep.* **2020**, *33*, 108528. [CrossRef] [PubMed]
35. Rossi, F.; Charlton, C.A.; Blau, H.M. Monitoring protein-protein interactions in intact eukaryotic cells by -galactosidase complementation. *Proc. Natl. Acad. Sci. USA* **1997**, *94*, 8405–8410. [CrossRef]
36. Smith, D.J.; Lapedes, A.S.; De Jong, J.C.; Bestebroer, T.M.; Rimmelzwaan, G.F.; Osterhaus, A.D.M.E.; Fouchier, R.A.M. Mapping the Antigenic and Genetic Evolution of Influenza Virus. *Science* **2004**, *305*, 371–376. [CrossRef]
37. Katzelnick, L.C.; Fonville, J.M.; Gromowski, G.D.; Arriaga, J.B.; Green, A.; James, S.L.; Lau, L.; Montoya, M.; Wang, C.; VanBlargan, L.A.; et al. Dengue viruses cluster antigenically but not as discrete serotypes. *Science* **2015**, *349*, 1338–1343. [CrossRef] [PubMed]
38. Edara, V.-V.; Pinsky, B.A.; Suthar, M.S.; Lai, L.; Davis-Gardner, M.E.; Floyd, K.; Flowers, M.W.; Wrammert, J.; Hussaini, L.; Ciric, C.R.; et al. Infection and Vaccine-Induced Neutralizing-Antibody Responses to the SARS-CoV-2 B.1.617 Variants. *N. Engl. J. Med.* **2021**, *385*, 664–666. [CrossRef]
39. McCallum, M.; Walls, A.C.; Sprouse, K.R.; Bowen, J.E.; Rosen, L.E.; Dang, H.V.; Marco, A.D.; Franko, N.; Tilles, S.W.; Logue, J.; et al. Molecular basis of immune evasion by the Delta and Kappa SARS-CoV-2 variants. *Science* **2021**, eabl8506. [CrossRef]
40. Tada, T.; Zhou, H.; Dcosta, B.M.; Samanovic, M.I.; Mulligan, M.J.; Landau, N.R. SARS-CoV-2 Lambda Variant Remains Susceptible to Neutralization by mRNA Vaccine-elicited Antibodies and Convalescent Serum. *bioRxiv* **2021**. Available online: https://www.biorxiv.org/content/10.1101/2021.07.02.450959v1.full (accessed on 29 October 2021). [CrossRef]
41. Planas, D.; Veyer, D.; Baidaliuk, A.; Staropoli, I.; Guivel-Benhassine, F.; Rajah, M.M.; Planchais, C.; Porrot, F.; Robillard, N.; Puech, J.; et al. Reduced sensitivity of SARS-CoV-2 variant Delta to antibody neutralization. *Nat. Cell Biol.* **2021**, *596*, 276–280. [CrossRef] [PubMed]
42. Steensels, D.; Pierlet, N.; Penders, J.; Mesotten, D.; Heylen, L. Comparison of SARS-CoV-2 Antibody Response Following Vaccination With BNT162b2 and mRNA-1273. *JAMA* **2021**, *326*, 1533–1535. [CrossRef] [PubMed]
43. Liu, J.; Liu, Y.; Xia, H.; Zou, J.; Weaver, S.C.; Swanson, K.A.; Cai, H.; Cutler, M.; Cooper, D.; Muik, A.; et al. BNT162b2-elicited neutralization of B.1.617 and other SARS-CoV-2 variants. *Nat. Cell Biol.* **2021**, *596*, 273–275. [CrossRef] [PubMed]
44. Barnes, C.O.; Jette, C.A.; Abernathy, M.E.; Dam, K.-M.A.; Esswein, S.R.; Gristick, H.B.; Malyutin, A.G.; Sharaf, N.G.; Huey-Tubman, K.E.; Lee, Y.E.; et al. SARS-CoV-2 neutralizing antibody structures inform therapeutic strategies. *Nature* **2020**, *588*, 682–687. [CrossRef] [PubMed]
45. Thomson, E.C.; Rosen, L.E.; Shepherd, J.G.; Spreafico, R.; Filipe, A.D.S.; Wojcechowskyj, J.A.; Davis, C.; Piccoli, L.; Pascall, D.J.; Dillen, J.; et al. Circulating SARS-CoV-2 spike N439K variants maintain fitness while evading antibody-mediated immunity. *Cell* **2021**, *184*, 1171–1187.e20. [CrossRef]
46. Starr, T.N.; Greaney, A.J.; Hilton, S.K.; Ellis, D.; Crawford, K.H.; Dingens, A.S.; Navarro, M.J.; Bowen, J.E.; Tortorici, M.A.; Walls, A.C.; et al. Deep Mutational Scanning of SARS-CoV-2 Receptor Binding Domain Reveals Constraints on Folding and ACE2 Binding. *Cell* **2020**, *182*, 1295–1310.e20. [CrossRef] [PubMed]
47. Motozono, C.; Toyoda, M.; Zahradnik, J.; Ikeda, T.; Saito, A.; Tan, T.S.; Ngare, I.; Nasser, H.; Kimura, I.; Uriu, K.; et al. An emerging SARS-CoV-2 mutant evading cellular immunity and increasing viral infectivity. *bioRxiv* **2021**. Available online: https://www.biorxiv.org/node/1882366.full (accessed on 29 October 2021). [CrossRef]
48. Yi, C.; Sun, X.; Lin, Y.; Gu, C.; Ding, L.; Lu, X.; Yang, Z.; Zhang, Y.; Ma, L.; Gu, W.; et al. Comprehensive mapping of binding hot spots of SARS-CoV-2 RBD-specific neutralizing antibodies for tracking immune escape variants. *Genome Med.* **2021**, *13*, 1–17. [CrossRef] [PubMed]
49. Zhang, L.; Mann, M.; Syed, Z.A.; Reynolds, H.M.; Tian, E.; Samara, N.L.; Zeldin, D.C.; Tabak, L.A.; Hagen, K.G.T. Furin cleavage of the SARS-CoV-2 spike is modulated by O-glycosylation. *Proc. Natl. Acad. Sci. USA* **2021**, *118*, e2109905118. [CrossRef]
50. Mlcochova, P.; Kemp, S.A.; Dhar, M.S.; Papa, G.; Meng, B.; Ferreira, I.A.T.M.; Datir, R.; Collier, D.A.; Albecka, A.; Singh, S.; et al. SARS-CoV-2 B.1.617.2 Delta variant replication and immune evasion. *Nat. Cell Biol.* **2021**, *599*, 114–119. [CrossRef] [PubMed]
51. Lubinski, B.; Frazier, L.E.; Phan, M.V.T.; Bugembe, D.L.; Tang, T.; Daniel, S.; Cotten, M.; Jaimes, J.A.; Whittaker, G.R. Spike protein cleavage-activation mediated by the SARS-CoV-2 P681R mutation: A case-study from its first appearance in variant of interest (VOI) A.23.1 identified in Uganda. *bioRxiv* **2021**. Available online: https://www.biorxiv.org/content/10.1101/2021.06.30.450632v2.full.pdf (accessed on 29 October 2021). [CrossRef]
52. Saito, A.; Irie, T.; Suzuki, R.; Maemura, T.; Nasser, H.; Uriu, K.; Kosugi, Y.; Shirakawa, K.; Sadamasu, K.; Kimura, I.; et al. Enhanced fusogenicity and pathogenicity of SARS-CoV-2 Delta P681R mutation. *Nature* **2021**, *9*. [CrossRef]
53. Duckert, P.; Brunak, S.; Blom, N.S. Prediction of proprotein convertase cleavage sites. *Protein Eng. Des. Sel.* **2004**, *17*, 107–112. [CrossRef]

54. Tian, S.; Huajun, W.; Wu, J. Computational prediction of furin cleavage sites by a hybrid method and understanding mechanism underlying diseases. *Sci. Rep.* **2012**, *2*, 261. [CrossRef]
55. Millet, J.K.; Whittaker, G.R. Host cell entry of Middle East respiratory syndrome coronavirus after two-step, furin-mediated activation of the spike protein. *Proc. Natl. Acad. Sci. USA* **2014**, *111*, 15214–15219. [CrossRef]
56. Coutard, B.; Valle, C.; de Lamballerie, X.; Canard, B.; Seidah, N.; Decroly, E. The spike glycoprotein of the new coronavirus 2019-nCoV contains a furin-like cleavage site absent in CoV of the same clade. *Antivir. Res.* **2020**, *176*, 104742. [CrossRef]
57. Dahms, S.; Hardes, K.; Steinmetzer, T.; Than, M.E. X-ray Structures of the Proprotein Convertase Furin Bound with Substrate Analogue Inhibitors Reveal Substrate Specificity Determinants beyond the S4 Pocket. *Biochemistry* **2018**, *57*, 925–934. [CrossRef] [PubMed]
58. Tian, S. A 20 Residues Motif Delineates the Furin Cleavage Site and its Physical Properties May Influence Viral Fusion. *Biochem. Insights* **2009**, *2*, BCI.S2049. [CrossRef]
59. Peacock, T.P.; Goldhill, D.H.; Zhou, J.; Baillon, L.; Frise, R.; Swann, O.C.; Kugathasan, R.; Penn, R.; Brown, J.C.; Sanchez-David, R.Y.; et al. The furin cleavage site in the SARS-CoV-2 spike protein is required for transmission in ferrets. *Nat. Microbiol.* **2021**, *6*, 899–909. [CrossRef]
60. Yadav, P.D.; Mohandas, S.; Shete, A.M.; Nyayanit, D.A.; Gupta, N.; Patil, D.Y.; Sapkal, G.N.; Potdar, V.; Kadam, M.; Kumar, A.; et al. SARS CoV-2 variant B.1.617.1 is highly pathogenic in hamsters than B.1 variant. *bioRxiv* **2021**. Available online: https://www.biorxiv.org/content/10.1101/2021.05.05.442760v1 (accessed on 29 October 2021).
61. Tang, T.; Jaimes, J.A.; Bidon, M.K.; Straus, M.R.; Daniel, S.; Whittaker, G.R. Proteolytic Activation of SARS-CoV-2 Spike at the S1/S2 Boundary: Potential Role of Proteases beyond Furin. *ACS Infect. Dis.* **2021**, *7*, 264–272. [CrossRef] [PubMed]
62. Hodcroft, E.B.; Domman, D.B.; Snyder, D.J.; Oguntuyo, K.Y.; Van Diest, M.; Densmore, K.H.; Schwalm, K.C.; Femling, J.; Carroll, J.L.; Scott, R.S.; et al. Emergence in late 2020 of multiple lineages of SARS-CoV-2 Spike protein variants affecting amino acid position 677. *medRxiv* **2021**. Available online: https://www.medrxiv.org/content/10.1101/2021.02.12.21251658v1 (accessed on 29 October 2021).
63. Scheepers, C.; Everatt, J.; Amoako, D.G.; Mnguni, A.; Ismail, A.; Mahlangu, B.; Wibmer, C.K.; Wilkinson, E.; Tegally, H.; San, J.E.; et al. The continuous evolution of SARS-CoV-2 in South Africa: A new lineage with rapid accumulation of mutations of concern and global detection. *medRxiv* **2021**. Available online: https://www.medrxiv.org/content/10.1101/2021.08.20.21262342v1 (accessed on 29 October 2021).
64. Daly, J.L.; Simonetti, B.; Klein, K.; Chen, K.-E.; Williamson, M.K.; Antón-Plágaro, C.; Shoemark, D.K.; Simón-Gracia, L.; Bauer, M.; Hollandi, R.; et al. Neuropilin-1 is a host factor for SARS-CoV-2 infection. *Science* **2020**, *370*, 861–865. [CrossRef] [PubMed]
65. Cheng, M.H.; Porritt, R.A.; Rivas, M.N.; Krieger, J.M.; Ozdemir, A.B.; Garcia, G.; Arumugaswami, V.; Fries, B.C.; Arditi, M.; Bahar, I. A monoclonal antibody against staphylococcal enterotoxin B superantigen inhibits SARS-CoV-2 entry in vitro. *Structure* **2021**, *29*, 951–962.e3. [CrossRef] [PubMed]
66. Rajah, M.M.; Hubert, M.; Bishop, E.; Saunders, N.; Robinot, R.; Grzelak, L.; Planas, D.; Dufloo, J.; Gellenoncourt, S.; Bongers, A.; et al. SARS-CoV-2 Alpha, Beta, and Delta variants display enhanced Spike-mediated syncytia formation. *EMBO J.* **2021**, *2*, e108944. [CrossRef]
67. Zhang, J.; Xiao, T.; Cai, Y.; Lavine, C.L.; Peng, H.; Zhu, H.; Anand, K.; Tong, P.; Gautam, A.; Mayer, M.L.; et al. Membrane fusion and immune evasion by the spike protein of SARS-CoV-2 Delta variant. *Science* **2021**, *374*, 1353–1360. [CrossRef] [PubMed]